



Soil carbon dioxide fluxes to atmosphere: the role of rainfall over CO₂ transport

Isabelle Delsarte, Grégory Cohen, Marian Momtbrun, Patrick Höhener,
Olivier Atteia

► To cite this version:

Isabelle Delsarte, Grégory Cohen, Marian Momtbrun, Patrick Höhener, Olivier Atteia. Soil carbon dioxide fluxes to atmosphere: the role of rainfall over CO₂ transport. *Applied Geochemistry*, 2021, 127, pp.104854. 10.1016/j.apgeochem.2020.104854 . hal-03087039

HAL Id: hal-03087039

<https://amu.hal.science/hal-03087039>

Submitted on 5 Jan 2021

HAL is a multi-disciplinary open access archive for the deposit and dissemination of scientific research documents, whether they are published or not. The documents may come from teaching and research institutions in France or abroad, or from public or private research centers.

L'archive ouverte pluridisciplinaire **HAL**, est destinée au dépôt et à la diffusion de documents scientifiques de niveau recherche, publiés ou non, émanant des établissements d'enseignement et de recherche français ou étrangers, des laboratoires publics ou privés.

Soil carbon dioxide fluxes to atmosphere: the role of rainfall to control CO₂ transport

Isabelle DELSARTE^{1*}, Grégory COHEN¹, Marian MOMTBRUN¹, Patrick Höhener² and

Olivier ATTEIA¹

¹ EA 4592 G&E, Bordeaux INP, 1 allée F. Daguin, 33607 Pessac, France

² Aix-Marseille Université - CNRS, Laboratoire Chimie Environnement UMR 7376, 3 place Victor Hugo, 13331 Marseille, France

*isabelle.delsarte@bordeaux-inp.fr

Abstract

In order to observe the relationships between the temporal variations of CO₂ surface and the CO₂ soil gas transport in soil profile before and during rainfall events, two experiments were conducted in a controlled natural environment at different time periods. The experiments consisted in injecting pure CO₂ in a lysimeter at 160 cm depth and simulating heavy rainfall event at its surface for 2 weeks. During the whole experiments, CO₂ gas concentrations and surface fluxes were continuously monitored. These measurements showed that the flux measured through the flux chamber were consistent with the concentration profiles. During simulated rainfall events, the concentrations and fluxes showed a clear change due to the presence of water on the top of the water profile. The results clearly show a significant decrease of CO₂ flux to atmosphere induced by rainfall infiltration and consequential release of the CO₂ present in the soil.

Keywords: CO₂ concentration, soil CO₂ flux, rainfall, soil gas concentration and fluxes monitoring

23 1. Introduction

24 The soil is the interface between the different environmental compartments (lithosphere,
25 the atmosphere...), where fluxes of water, particles and gas are constantly exchanged. Due to
26 past and current human activities, the composition of these fluxes was significantly altered, that
27 imposes a threat to the environment and human health. During the last decades, special attention
28 has been paid to gas exchanges at the soil-atmosphere interface. Indeed, the need to understand
29 and monitor gas fluxes is ubiquitous in many areas of human activity. For example, on the
30 carbon capture and storage sites, the monitoring of CO₂ fluxes is necessary to detect and
31 quantify eventual leakages to the environment (Bernardo and Vries, 2011; Beaubien et al.,
32 2013; Schroder et al., 2016; Elío et al., 2016). Following landfill gas emissions across the
33 surface of landfills is also essential. Indeed, the landfill gas is ranked as the third highest source
34 of global anthropogenic methane emissions (Yang et al., 2015) and contributes also to large
35 CO₂ emissions. Another example concerns the contaminated sites, where measurement soil gas
36 fluxes are often required as part of human health risk assessment of the site or when
37 implementing a risk-based corrective approach (Hers et al., 2004).

38 Gas flux at the soil-atmosphere interface, can be directly measured using flux chambers
39 methods (Bornemann, 1920; Klenbusch, 1986). These techniques are based on the
40 measurement of the compound concentration increase inside an open-bottom chamber set up
41 on the soil surface. The gas flux is then calculated by relating the concentration increase during
42 a given time to the chamber volume and the concerned soil surface area. Due to the low cost of
43 this non-intrusive method which is easy to set up, it has been widely used (Cotel et al., 2015;
44 Elío et al., 2016; Jassal et al., 2005; Matthias et al., 1980; Norman et al., 1997; Reinhart et al.,
45 1992; Rochette and Hutchinson, 2005; Viveiros et al., 2008). Indeed, this technique allows to
46 carry out *in situ* measurements quickly and on a large number of points compared to other
47 techniques (Schroder et al., 2016).

48 However, due to the soil heterogeneity resulting from the spatial and temporal
49 variability of the physico-chemical soil properties such as moisture, the instantaneous fluxes
50 measured in practice do not allow to easily determine the long term transport of vapours to the
51 atmosphere (Bekele et al., 2014). Several authors observed seasonal variations of gas surface
52 fluxes or soil gas concentrations (Elío et al., 2013; Kim et al., 2019). Indeed, these researchers
53 observed the dependence of CO₂ fluxes with soil moisture variations which are likely to govern
54 soil gas transport processes. Petersen et al. (1996) and Choi et al. (2005) observed that
55 trichloroethene (TCE) gas-phase diffusive fluxes at soil surface were also sensitive to soil-water
56 content modifications. Moisture content in the subsurface modifies the pore volume available
57 for gas transport (Risk et al., 2002; Tillman and Smith, 2004; Palaia et al., 2018). Moisture
58 content impacts the transport of gas phase in the soil by modifying soil tortuosity as well as the
59 effective diffusivity and the dissolved quantity of the concerned compound in the aqueous phase
60 (Conant et al., 1996; Hers et al., 2000; Jassal et al., 2005). In the literature, there is still an
61 ongoing discussion about the different formulae used to link soil water content to the effective
62 tortuosity (Hers et al., 2000; Werner et al., 2004). The heterogeneous distribution of soil
63 moisture content has also a direct effect on subsurface gas concentration profile (Shen et al.,
64 2013). Wetter soil layers could therefore have different effects such as reducing the gas
65 diffusion from the source to the atmosphere or, conversely, increasing surface fluxes. It was
66 also shown that rainfall duration, intensity, frequency and spatial variability has direct influence
67 on gas fluxes (Fa et al., 2015; Lelli and Raco, 2017; Ma et al., 2012; Seo et al., 2020;
68 Tommasone Pascale et al., 2015). In their study, Viveiros et al. (2008) showed that depending
69 on the intensity of the rainfall, the soil CO₂ fluxes are different. Tommasone Pascale et al.
70 (2015) observed the influence of rainfall events on soil radon (²²²Rn) concentration and
71 concluded that time evolution of soil ²²²Rn activities are markedly dependent on the rainfall
72 history of the site.

73 While there is a general agreement on the importance of soil water content, there has
74 been, to our knowledge, limited quantitative analysis related to its influence (Hers et al., 2000;
75 Oh et al., 2019; Shen et al., 2013). Even if some field and / or numerical studies have considered
76 some temporal effects on soil gas transport, a full explanation of the influence of rainfall events
77 on soil gas concentrations and fluxes is still not available (Viveiros et al., 2008; Lewicki et al.,
78 2009; Shen et al., 2012). However, understanding how these short and/or long-term variations
79 modify soil gas transport processes is of major importance for precisely quantify long term gas
80 fluxes at monitoring sites.

81 Therefore, the main objective of this study is to understand the relationships between
82 the temporal variations of gas surface fluxes and the soil gas transport in soil profile before and
83 during rainfall events. To this end, two experiments were conducted in a controlled natural
84 environment. These experiments consisted in injecting pure CO₂ in a lysimeter and simulating
85 rainfall event at its surface. During the whole experiments, CO₂ soil gas concentrations and
86 surface fluxes were continuously monitored. The impact of natural rainfall events of different
87 intensities and frequencies on CO₂ fluxes at the soil-atmosphere interface were also observed.

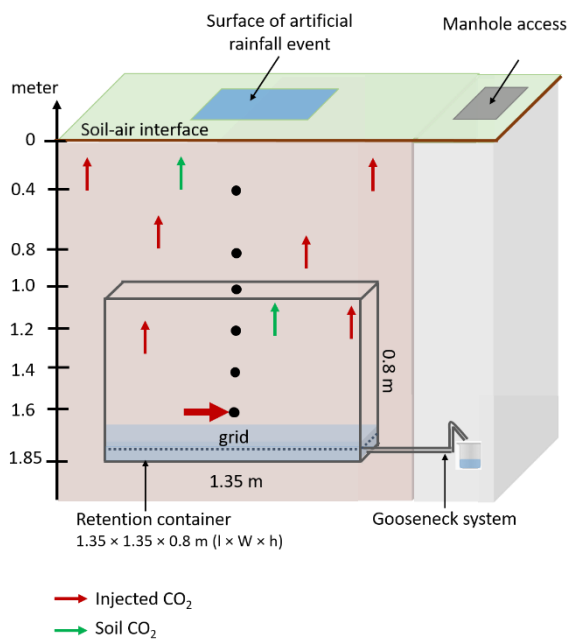
88 2. Materials and methods

89 2.1.Lysimeter description

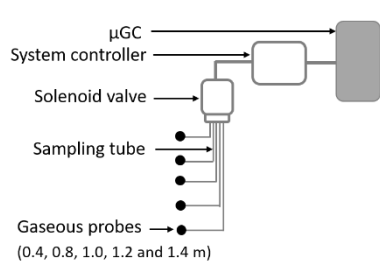
90 The experiments were conducted in a lysimeter, a controlled natural environment
91 (Figure 1). This lysimeter was set up in August 2014. Soil digging was conducted thanks to a
92 mechanical shovel which removed and separated sequentially 50 cm depth soils layers until
93 1.85 m depth. The retention tank ($l \times w \times h = 1.35 \times 1.35 \times 0.8 \text{ m}$) was then set-up. At the
94 bottom of the tank, a grid was added allowing an easier water recovery. Moreover, a gooseneck
95 system, connected to the bottom of the retention tank allows the control of the piezometric level
96 and the quantification of outflowing water. After the set-up of the retention tank, the soil was
97 manually put back in place backward in order to respect as much as possible the original soil

98 configuration. Each soil layer of 10 cm height was compacted. In the centre of lysimeter, six
 99 gas probes were set up during this backfill, placing them at specific depths (0.4, 0.8, 1.0, 1.2,
 100 1.4 and 1.6 m depth) (Figure 1). To avoid vertical preferential paths, their tubes were placed in
 101 the ground horizontally until the manhole. Thus, the soil removed during the lysimeter
 102 installation was returned to respect as much as possible its initial structure. The soil matrix is
 103 an alluvial sand from the Aquitaine basin (France). Moreover, the soil does not contain calcite
 104 (<1%) over the entire vertical profile of the lysimeter and the CEC capacity varies from 15
 105 mmol/kg at 20 cm to 1-2 at 1 m depth.

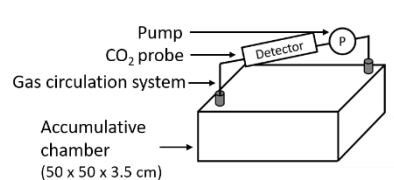
A- Vertical section:



B- Automated measurement system:



C- Passive flux chamber



D- Horizontal section:

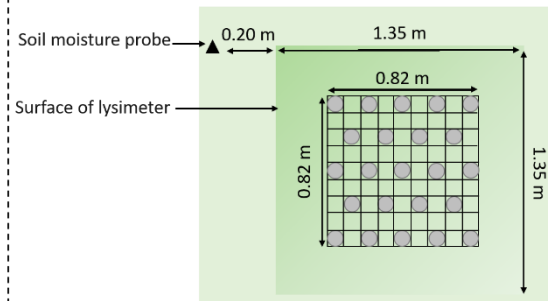


Figure 1. General description of the lysimeter. A- Vertical section of the lysimeter: a grid rested on the bottom of the tank and allowed the porous medium to be separated from the water. The black dots represent the location of the gas probes. B- Automated measurement system for continuous monitoring of CO₂ concentrations in the soil. C- Schematic of passive flux chamber used to determine surfaces fluxes. D- Horizontal section of the lysimeter: the blue and grey dots represents the location of the piezometer and the tubes used for artificial the rainfall event, respectively.

107 2.2.Hydrological properties of porous media

108 2.2.1. Determination of soil porosity and water content by soil coring

109 The initial water content, the residual water saturation and the porosity of the porous
110 medium were experimentally determined. Soil cores were taken from the experimental plot next
111 to the lysimeter at 0.2, 0.5 and 1.0 m depth. The sampling tool consists in a sampling tube on
112 which is added a corer (S x L: 11.95 x 14.8 cm²). A pilot hole is previously made with a manual
113 auger to the desired depth. The tube is then driven into the ground either directly or with a
114 sledgehammer. Soil cores were first slowly saturated with tap water for 24 h before being placed
115 in the oven at 105°C for 24 h (Wilke, 2005). At every step, soil cores were weighted.

116 2.2.2. Transient water content measurement

117 Soil moisture content was determined by using moisture probes (120 cm; Drill & Drop
118 Probe, SDI-12, Sentek) composed by ten moisture sensors. Thus, soil moisture was measured
119 every 10 cm from 7 to 97 cm depth. To avoid preferential gas flow and damage of gas sample
120 probes, this probe was set up 20 cm next to the lysimeter (Figure 1). The soil matrix at this
121 emplacement is the same as the one inside the lysimeter. The soil moisture probes were
122 calibrated *in situ* by an analysis of their temporal signal variations with respect to the cumulative
123 amount of water infiltrated during the artificial rainfall event.

124 2.3.CO₂ soil gas concentration measurements

125 CO₂ soil gas concentrations were continuously monitored with the use of a custom

126 automated system. This automated system is composed of a micro-GC (CP-4900, Varian Inc.),
127 a system controller (M3 Essential extensibles, Crouzet) and a solenoid valve (EMHMA-CE,
128 Vici Valco) directly connected to the five soil gas probes (0.4, 0.8, 1.0, 1.2 and 1.4 m depth)
129 (Figure 1). The micro-GC is equipped with a PPQ column to separate CO₂. The general relative
130 uncertainty for the quantification of CO₂ with this method is less than 5%. Tubes of 2.50 m

131 with an inner diameter of 0.5 mm were used to connect each gas probe to the automated system.
132 For each analysis, a gas sample of 70 mL was collected from the soil by micro-GC pumping
133 system. The dead volumes of the gas tubes were taken under consideration to determine the
134 optimal sampling volume.

135 2.4. Gas flux monitoring at the soil surface using a flux chamber

136 A Passive Flux Chamber (PFC) (50 x 50 x 3.5 cm (L x W x H)) was used to monitor
137 CO₂ gas fluxes at the centre of the lysimeter surface (Figure 1). A sealed pumping system with
138 a flowrate of about 500 mL min⁻¹ allows gas circulation from the accumulation chamber to the
139 detector and its homogenization inside the PFC. The CO₂ concentrations were measured with
140 a CO₂ probe (GMT222 Vaisala) placed in the PFC gas circulation system. To correct the CO₂
141 probe values, an intercomparison with the micro-GC was realized. This step was realized on
142 several CO₂ concentrations (Information is available in the Supplementary information).

143 The soil surface CO₂ gas fluxes (F_{CO_2} in g m⁻² min⁻¹) were calculated during the transient
144 state of gas transfer in the flux chamber headspace as follows (Matthias et al. 1980):

145
$$F_{CO_2} = \frac{V_{ch}}{A_{ch}} \times \frac{dC}{dt} \quad (1)$$

146 Where dC (g m⁻³) is the variation of the CO₂ vapour concentration in the chamber during
147 dt (min), V_{ch} (m³) is the net volume of the chamber, and A_{ch} (m²) the covered soil surface area.

148 Based on the principle of gas accumulation within the chamber, the initial slope of the
149 measured gas concentration-time curve is generally used to quantify the time derivative of Eq.
150 (1) (Cotel et al. 2015).

151 Uncertainties in the experimental CO₂ mass fluxes measured with this flux chamber
152 were calculated according to the method used by Cotel et al. (2015). Thus, uncertainties in the
153 flux measurements were determined using a total derivative expansion for correlated variables
154 of F_{CO_2} :

155
$$\frac{\Delta F_{CO_2}}{F_{CO_2}} = \sqrt{\left(\frac{\Delta(dC/dt)}{dc/dt}\right)^2 + \left(\frac{\Delta V_{ch}}{V_{ch}}\right)^2 + \left(\frac{\Delta A_{ch}}{A_{ch}}\right)^2} \quad (2)$$

156 Considering uncertainties of 5%, 4% and 8% for CO₂ detector measurements, PFC section and
157 volume, respectively, the total uncertainty in the measured fluxes is about 10.25%.

158 2.5. Experimental conditions

159 The same experiment was realized at two different times of the year, in February and
160 October 2019. The timeline of both experiments is presented in Figure 2. For each experiment,
161 the CO₂ injection began at day 0. When the CO₂ concentration gradient was stabilized, an
162 artificial rainfall event was realized at 8.6 d for the 1st experiment and at 6 d for the second (cf.
163 2.5.2). For the 2nd experiment, a natural rainfall event followed the artificial one at 9 d. During
164 the experiments, the atmospheric pressure varied between 1018 and 1031 hPa for the 1st
165 experiment and between 992 and 1023 hPa for the 2nd experiment.

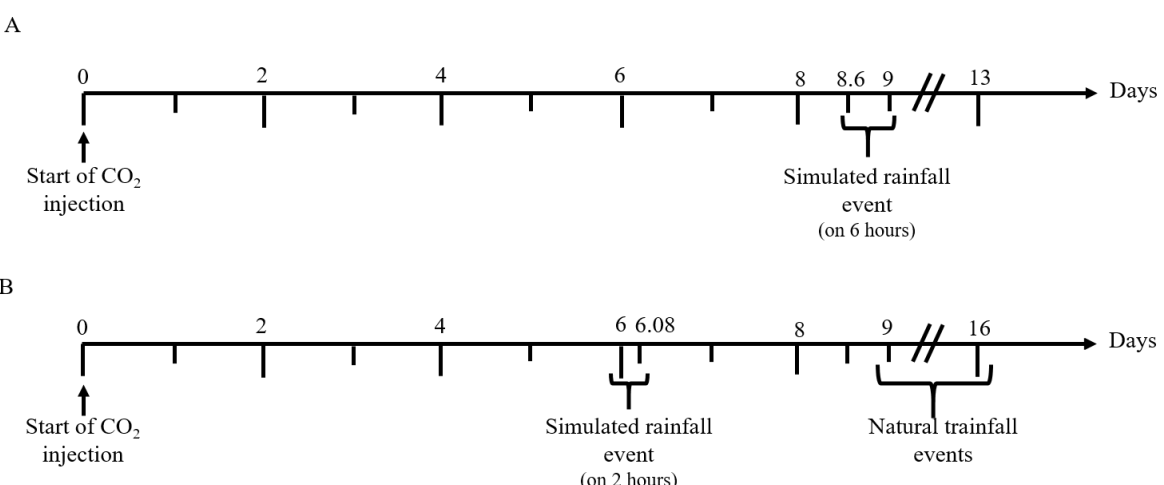


Figure 2. Timelines of the experiment realized in February 2019 (A) and in October 2019 (B).

166

167 2.5.1. Gas injection conditions

168 The gas injection was conducted with a bottle of CO₂ (99.7% Air Liquide) equipped
169 with a flow controller set at about 0.3 L.min⁻¹. The gas was injected inside the retention tank at
170 160 cm depth of the lysimeter for 2 weeks.

171 2.5.2. Artificial rainfall event

172 For the two experiments, an intense rainfall event of about 100 mm of tap water was
173 simulated during respectively 6 h and 2 h. The rainfall event was conducted in the centre of the
174 lysimeter over a surface of 0.82×0.82 m (0.67 m 2) leading to a total of 69 L. On this surface,
175 23 tubes (inner diameter: 8 cm; H: 15 cm) were placed regularly on a regular mesh (Figure 1)
176 and pressed 2 cm deep. These tubes allowed the homogeneous injection of tap water in soil (12
177 x 250 mL / tube). The water was recovered at the outlet of the lysimeter through the gooseneck
178 system (Figure 1). During the 2nd experiment, the same amount of water was injected in the
179 centre of the lysimeter and an equivalent artificial rainfall event was also realized around the
180 moisture probe. The rainfall event around the latter was conducted over a surface of 0.63 x
181 0.63 m leading to a total of 42 L. Given the proximity of the probe to the lysimeter,
182 approximately 50% of the quantity of water injected could be collected at the outlet of the
183 lysimeter, i.e. the equivalent of 90 L.

184 2.6.Calculation of the CO₂ mass balance

185 The domain considered for determining the approximate mass balance is the surface
186 covered by the artificial rainfall event (0.672 m 2) across a depth of 80 cm, equivalent to a
187 volume of 538 L. This domain is divided over depth in 16 equal subdomains ($l \times w \times h = 82 \times$
188 82×5 cm). Each subdomain was characterised by the porosity, soil moisture content, gas phase
189 volume as well as CO₂ soil concentrations in aqueous and gaseous phase.

190 According to porosities determined by soil coring method, a porosity of 0.33 was
191 considered for the subdomains located between 0 to 0.5 m depth and 0.29 for the others located
192 between 0.5 to 0.8 m depth. Soil moisture content of each subdomains was estimated based on
193 soil moisture profile data allowing to calculated water phase volume ($V_{aqueous\ phase}$):

194 $V_{aqueous\ phase} = \theta_{water} \times V_{subdomain}$ (3)

195 Where Θ_{water} (-) is the volumetric soil water content and $V_{subdomain}$ (L) is the volume of the
196 subdomain.

197 The gas phase volume was then calculated as follows:

198
$$V_{gaseous\ phase} = (\theta - \theta_{water}) \times V_{subdomain} \quad (4)$$

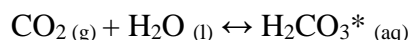
199 Where θ (-) is the total connected porosity.

200 CO₂ mass in the gaseous phase in each subdomain was determined based on CO₂ profiles
201 data (Figure 5) and linear interpolation method. Assuming that in the soil the equilibrium
202 between aqueous and gaseous phase was instantaneous, Henry's law was used to calculate the
203 CO₂ mass in the aqueous phase ($m_{aqueous\ phase}$):

204
$$m_{aqueous\ phase} = (C_{gaseous\ phase} \times H^{cc}) \times V_{aqueous\ phase} \quad (5)$$

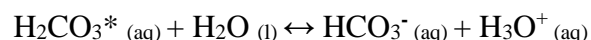
205 Where, H^{cc} is the dimensionless Henry solubility (C_a/C_g). According to Sander et al. (2011) the
206 H^{cc} value is 0.818 at 25°C.

207 However, the H^{cc} value can change according to the buffering capacity (or alkalinity) of
208 soil water which is the water capacity for solutes it contains to react with and neutralize acid.
209 Thus, in contact with water, H₂O (l) and CO₂ (g) form a carbonic acid molecule H₂CO₃ (aq)
210 according to the carbonation reaction:

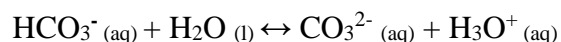


212 Where H₂CO_{3*} represents the total concentration of dissolved CO₂ and H₂CO₃.

213 As H₂CO₃ (aq) is an acid, it reacts to form a bicarbonate ion HCO₃⁻ (aq) and a solvated
214 proton H₃O⁺ (aq):



216 Then:



218 The previous reactions increase the apparent solubility of CO₂. These dissolutions can
 219 also be increased in presence of calcite. However, the Bernard calcimeter method showed that
 220 the level of calcite in the soil studied was inferior to the quantification level (0.1%) (Rodier,
 221 1976). Thus, from the alkalinity, pH and CO₂ added in the media, an apparent Henry constant
 222 (H_{app}^{cc}) can be calculated. Before and during the CO₂ injection (at steady state), alkalinity
 223 measurements were realized by titration method (Table 1) on the water recovered at the outlet
 224 of the lysimeter (Rodier, 1976). Alkalinity at 0.4 m and 0.8 m was estimated based on CO₂
 225 concentration profile at steady state (Figure 5) and alkalinity in the outflowing water using a
 226 linear interpolation (Table 1). According to this method, the average value of H_{app}^{cc} estimated is
 227 1.151 at 15°C.

228 Table 1. Parameters of the water recovered at the outlet of the lysimeter before and during the
 229 CO₂ injection at steady state.

Experiment		at 0 d	At steady state		
Soil	Depth (m)	1.85	1.85	0.8	0.4
	CO ₂ gas concentration (% Vol CO ₂)	0.30	99.70	20.73	4.55
	CO ₂ gas concentration added ^a	/	99.40	20.43	4.25
Aqueous phase		pH	7.39	6.41	
		Alkalinity (mol L ⁻¹)	0.0034	0.0256	/
		H ₂ CO ₃ concentration (mol L ⁻¹) ^a	0.0004	0.0259	/
		HCO ₃ ⁻ concentration added (mol L ⁻¹) ^b	/	0.0222 ^a	0.0046
		H ₂ CO ₃ concentration added (mol L ⁻¹) ^c	/	0.0255 ^b	0.0052

230 ^a 10^(pKa x log([HCO₃⁻] – pH)) with pKa = 6.415 at 15°C

231 ^b [HCO₃⁻] added = ([HCO₃⁻] at steady state - [HCO₃⁻] at 0 d) x% CO₂ gas concentration added

232 ^c [H₂CO₃*] added = ([H₂CO₃*] at steady state - [H₂CO₃*] at 0 d) x% CO₂ gas concentration added

233

234 3. Results

235 3.1. Artificial rainfall event monitoring

236 Figure 3 shows the evolution of soil moisture content as a function of depth at different
 237 periods: before and during the artificial rainfall event. For the 2nd experiment, the initial soil
 238 moisture content was different than for the 1st experiment (Figure 3).

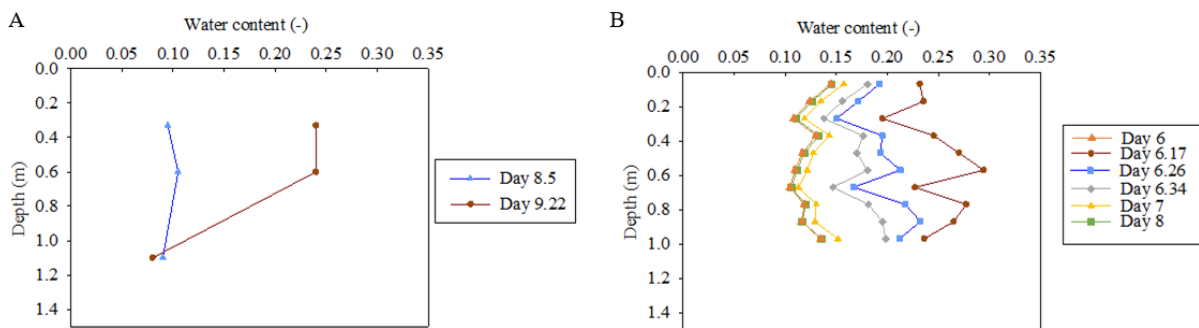


Figure 3. Spatial variation along vertical profile for soil moisture during and after the artificial rainfall event in February 2019 (A) and October 2019 (B) experiments.

239

240 Indeed, initial moisture content was in average of 0.097 for the February experiment
 241 and 0.12 for the 2nd experiment. Even if, water content varies in function of the depth, a
 242 consistent evolution of the profiles was observed during and after the rainfall event.

243 Figure 4 presents the cumulative outflow of water recovered at the outlet of the
 244 lysimeter. Two days after the artificial rainfall event, only 50% of the water amount injected
 245 was collected for the 1st experiment while this value was 92% for the 2nd experiment for the
 246 same duration. This difference may be linked to initial soil moisture content which was higher
 247 during the 2nd experiment (Figure 3).

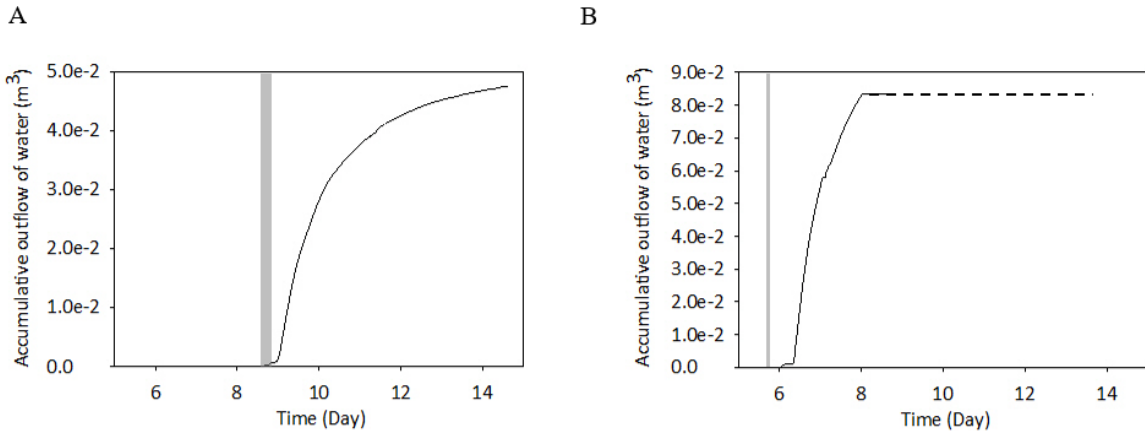


Figure 4. Cumulative outflow obtained during and after the artificial rainfall event in February 2019 (A) and October 2019 (B). The artificial rainfall events are highlighted with a grey area. The dotted lines indicate a data acquisition problem.

248

249 3.2. Soil CO₂ concentrations

250 Figure 5 presents the evolution of CO₂ soil gas concentrations as a function of depth at
251 different periods during the gas injection, until CO₂ profile stabilization. Measures were
252 realized before the CO₂ injection for baseline data. The CO₂ profiles obtained were like that
253 presented on Figure 5 at day 0 with a low CO₂ content ≈ 0.3 vol %. During the injection, CO₂
254 content between 0.4 and 1.4 m depth respectively increased until 5 and de making the CO₂
255 produced by the soil respiration negligible.

256 The CO₂ concentration at 0 m depth corresponds to the atmospheric concentration of
257 CO₂. For the first experiment, the CO₂ stabilization in the soil occurred about 4 days after the
258 injection began (Figure 5-A). For the second experiment, the stabilization occurred later, about
259 5-6 days after the injection started. Indeed, even if the overall profile seems to be stable at day
260 4, CO₂ concentration at 0.4 m depth still varied after day 4 in the 2nd injection (Figure 5-B).
261 Moreover, during the injection, a change of slope at 0.8 m depth was observed. Due to its
262 density, CO₂ gas (1.83 instead of 1.21 kg m⁻³ for air), may have accumulated in the lysimeter,
263 *i.e.* between 1.05 and 1.85 m depth, and the concentrations at 0.8 m may be influenced by dense
264 CO₂ flowing laterally from the lysimeter to the surrounding soil. This may explain the change

265 of CO₂ concentration slope observed at 0.8 and 0.4 m. Indeed, compared to diffusion, the
 266 density effect can be neglected only for very low concentrations. Thus, the interpretation of
 267 obtained results focused above all on the first 0.8 m of the lysimeter.

268

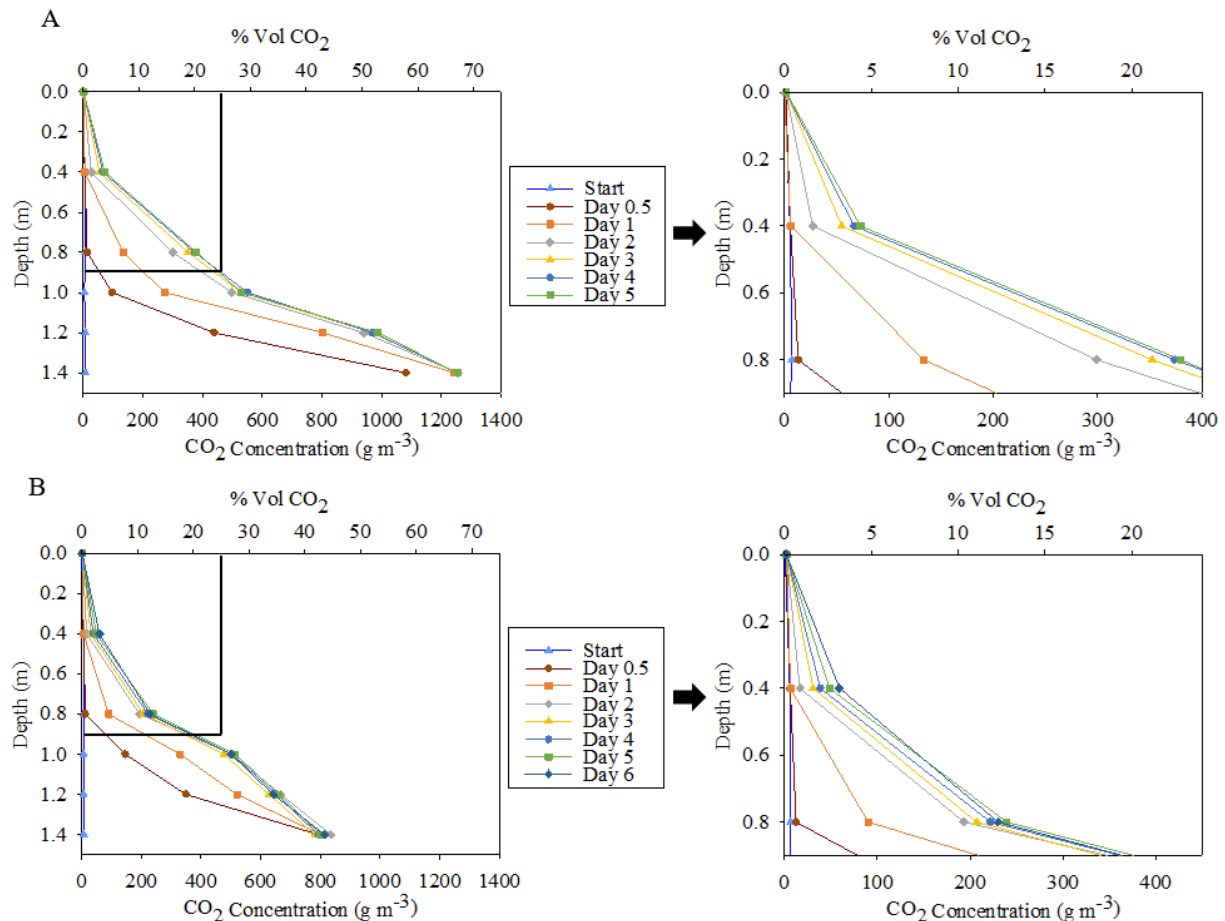


Figure 5. Evolution of CO₂ concentration profile at different period during the CO₂ injection in February 2019 (A) and in October 2019 (B). For A and B, the figure on the right is the inset of the figure on the left.

269 The temporal evolution of CO₂ soil gas concentrations is presented in Figure 6. In the
 270 left part of each graph, the increase of CO₂ soil concentrations is clearly observed during the
 271 beginning of the injection. The CO₂ gas concentrations at 0.4 and 0.8 m depth respectively
 272 increased to 80 and 380 g m⁻³ for the February experiment and to 50 and 230 g m⁻³ for the 2nd
 273 experiment. The grey part of graphs related to rainfall events will be described below.

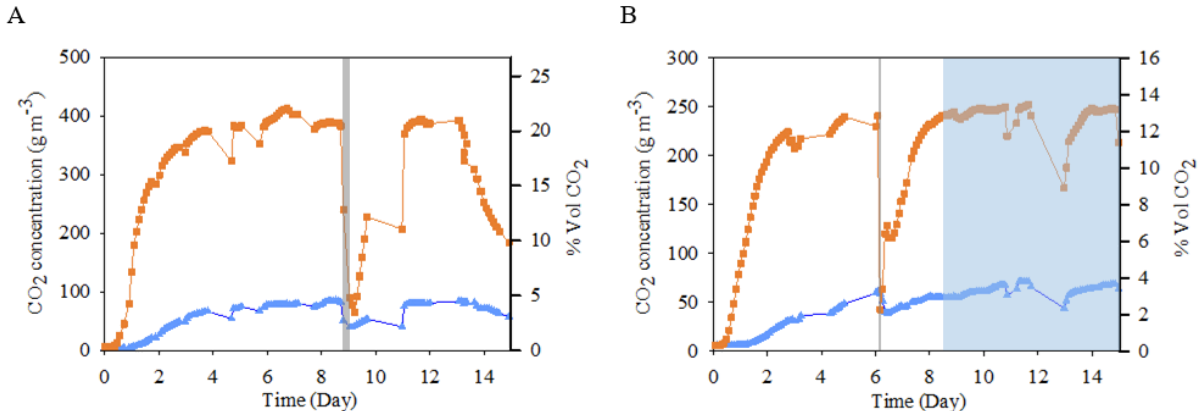


Figure 6. Times series for CO₂ soil gas concentrations measured at 0.4 (blue dots) and 0.8 m (orange dots) depth, in the centre of the lysimeter during the CO₂ injection in February 2019 (A) and in October 2019 (B). The artificial and natural rainfall events are underlined by a grey and blue area, respectively.

274

275 After the artificial rainfall event, the CO₂ profiles showed a significant modification
 276 linked to the presence of water at the top of the lysimeter. In fact, a clear decrease of CO₂ gas
 277 concentrations was observed, especially at 0.8 m depth (Figure 6 and 7). During the 1st
 278 experiment, the CO₂ concentration at this depth decreased rapidly from 388 to 65 g m⁻³. This
 279 minimum CO₂ concentration was measured 14 h after the beginning of the rainfall event and
 280 represents a 5.9-fold decrease (Figure 7). Then, CO₂ concentrations increased and reached their
 281 previous concentrations after two days. For the 2nd experiment, the CO₂ minimum concentration
 282 was reached faster than for the 1st experiment. Indeed, the CO₂ concentration at this depth
 283 decreased rapidly from 240 to 42 g m⁻³. This minimum CO₂ concentration was measured 4 h
 284 after the beginning of the rainfall event and represents a 5.6-fold decrease. Then, the CO₂
 285 profiles returned to the steady state after 2.75 and 2 days for 1st and 2nd experiment, respectively
 286 (Figure 7).

287 The CO₂ gas concentrations variations can be analysed in relation with soil moisture
 288 content change for the second rainfall event (Figure 3). The highest soil moisture contents were
 289 observed at 6.17 d when the CO₂ gas concentration at 0.8 m depth was the lowest. Moreover,

290 the moisture content profile turned back to steady state after 2 days as for CO₂ concentration
 291 profile (Figure 3 and 7).

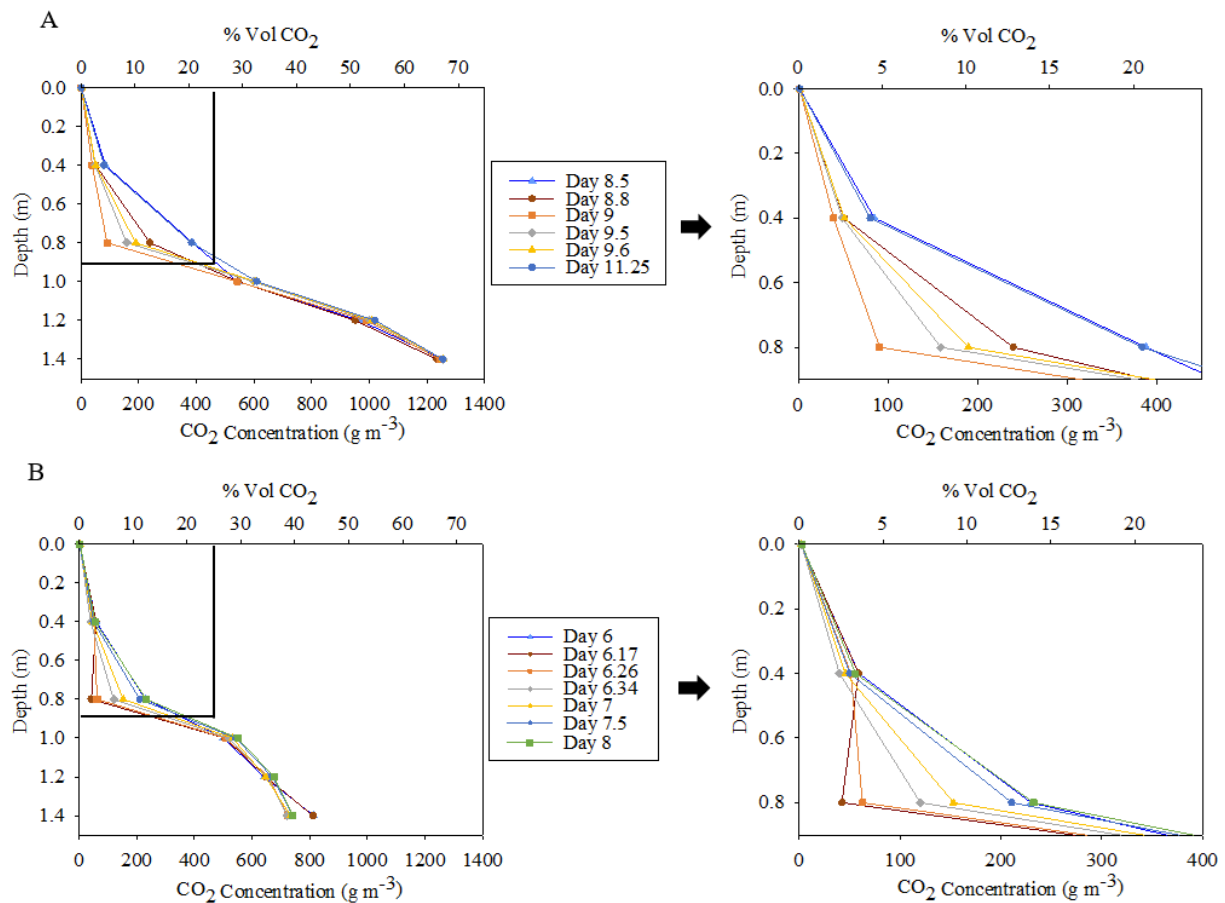


Figure 7. Evolution of CO₂ concentration profile at different period after the rainfall event, at 9 d for February 2019 (A) and at 6.08 d for October 2019 (B). For A and B, the figure on the right is the inset of the figure on the left.

292

293 3.3. CO₂ soil surface fluxes

294 The temporal evolution of CO₂ fluxes at lysimeter surface are presented in Figure 8. For
 295 the 1st experiment, the measured CO₂ fluxes increased until a stabilization around 35 mg m⁻²
 296 min⁻¹ which occurred about 5 days after injection began. For the 2nd experiment, the measured
 297 CO₂ fluxes increase until about 40 mg m⁻² min⁻¹. The fluxes measured across the surface were
 298 greatly inferior compared to the injected CO₂ flux because part of injected CO₂ escapes laterally
 299 and another part accumulates at depth.

300 After the artificial rainfall events, a significant decrease of CO₂ fluxes was noticed for
 301 both experiments. They dropped from 35 to below 10, and from 40 to 1 mg m⁻² min⁻¹ for 1st and
 302 2nd experiment (Figure 8), respectively. After these events, the CO₂ fluxes previously obtained
 303 at steady state were not reached again, while the soil CO₂ concentrations reached back their
 304 original values (Figure 7).

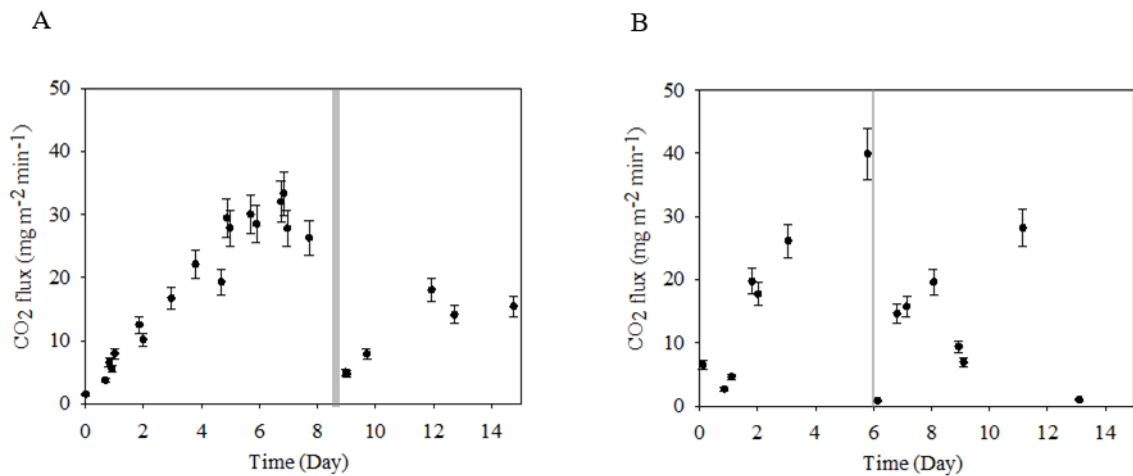


Figure 8. Times series of CO₂ soil surface fluxes, in the center of the lysimeter during the CO₂ injection in February 2019 (A) and in October 2019 (B). The artificial rainfall events are highlighted with a grey area.

305

306 3.4. CO₂ mass balance

307 To understand the influence of rainfall events on surface CO₂ gas fluxes, an approximate
 308 mass balance was calculated for both experiments. This mass balance is based on CO₂ profiles
 309 data obtained at the steady state (at 8.5 d and 6 d for event 1 and 2, respectively) and after the
 310 artificial rainfall events (at 9.22 d for event 1 and at 6.17 and 6.34 d for event 2) (Table 2),
 311 considering the surface covered by the artificial rainfall event (0.67 m²) across a depth of 80 cm.
 312 CO₂ mass in the aqueous phase was calculated with a standard H^{cc} value (Sander et al., 2011)
 313 and H_{app}^{cc} determined according to the alkalinity data.

314

315

316 Table 2. Estimated mass balance between the end of steady state of CO₂ profile and the end of
 317 the artificial rainfall event.

Zone characteristics					
		1st		2nd	
Media	Experiment	At steady state	After artificial rainfall event	At steady state	After artificial rainfall event
		at 8.5 d	at 9.22 d	at 6 d	at 6.17 d at 6.34 d
Soil	Volume of soil gaseous phase (L)	118.31	46.46	105.59	33.65 89.57
	Volume of the soil aqueous phase (L)	51.87	123.72	64.59	136.53 80.61
	CO ₂ mass in the gaseous phase (g)	16.55	1.82	9.99	1.3 4.16
	CO ₂ mass in the aqueous phase with H ^{cc} = 0.818 (g)	6.70	3.92	4.97	4.96 4.17
	CO ₂ mass in the aqueous phase with H ^{cc} = 1.151 (g)	9.43	5.52	6.99	6.98 5.86
Interface soil/air	CO ₂ Flux (mg m ⁻² min ⁻¹)	29.4 ± 3.8	5.69 ± 0.74	39.9 ± 5.19	0.79 ± 0.1 4.8 ± 0.62
	CO ₂ flow (g min ⁻¹)	0.020	0.004	0.027	0.0005 0.003
Soil	Mass Balance c	1st		2nd	
		9.22 d - 8.5 d		6.17 d - 6 d 6.34 d - 6.17 d	
	Δ CO ₂ mass in the gaseous phase (g)	-14.73		-8.69 2.86	
	Δ CO ₂ mass in the aqueous phase with H ^{cc} = 0.818 (g)	-2.78		-0.01 -0.79	
Interface soil/air	Δ CO ₂ mass in the aqueous phase with H ^{cc} = 1.151 (g)	-3.91		-0.01 -1.12	
	Δ CO ₂ mass (g)	16.59 ± 2.16		6.48 ± 0.84 0.66 ± 0.9	

318 ^aDetermined according to CO₂ concentration profile at steady state

319 ^bDetermined according to CO₂ concentration profile after the artificial rainfall event

320

321 During the 1st experiment, at steady state (8.5 d), the considered soil volume contained
 322 between 23.25 and 29.95 g of CO₂ with 16.55 g gaseous phase and between 6.70 and 13.40 g
 323 in aqueous phase. After the artificial rainfall event, at 9.22 d, the total CO₂ mass contained in
 324 considered soil volume decreased drastically. Indeed, the soil only contained between 5.74 and
 325 9.61 g (about 3.6 times less than at steady state) with 1.82 g gaseous phase and between
 326 3.92 and 7.79 g in aqueous phase. According to this mass balance, the mass of CO₂ lost in the
 327 gas phase between 8.5 and 9.22 d would have been moved to the atmosphere at the top of the
 328 investigated volume. In fact, according to CO₂ flux measurements, the CO₂ amount emitted at
 329 the soil/air interface during this period was 16.59 ± 2.16 g, corresponding rather well to the
 330 mass of CO₂ lost in the gas phase of about 14.73 g (Table 2). Concerning, the CO₂ amount in
 331 aqueous phase between these two states, it did not increase significantly, even if the quantity of

332 water injected at the soil surface (about 69 L) was localised in the investigated volume. Indeed,
333 the volume of the soil aqueous phase was 51.9 L at 8.5 d and 123.7 L at 9.22 d.

334 The same observations were done for the 2nd experiment. Indeed, CO₂ mass decreased
335 after the artificial rainfall event (6.17 d) by a factor of 2.1. The CO₂ amount in aqueous phase
336 did not significantly vary. The mass balance also shows that the mass of CO₂ lost in the gas
337 phase between 6.0 and 6.17 days is equivalent to the one lost at the top of the lysimeter. After
338 day 6.34 of this 2nd experiment, a return at steady state conditions is observed (11 d) (Figure 7).
339 Indeed, the water added begun to flow out of the investigated volume and the CO₂ mass in the
340 gaseous phase begun to increase. A decrease, between 0.79 and 1.57 g of CO₂ in the aqueous
341 phase is observed (Table 2).

342 3.5.Influence of natural rainfall events

343 The temporal evolution of precipitations and soil moisture content after the 2nd rainfall
344 event are presented in Figure 9. The rainfall events modify directly soil moisture content even
345 during a light and short-term rain. However, the depth of soil moisture modification varies
346 according to the rainfall intensity and duration. For example, during the light and short-term
347 rains between 20 and 22 d, a little increase of soil moisture could be only observed at 0.07 m
348 depth whereas during the light and longer-term rainfall events (18 d - 19 d), the water contents
349 were modified at 0.07 and 0.37 m depth (Figure 9-C and D). During the heavy natural rainfall
350 events highlighted in blue (Figure 9-C), soil moisture increased at every depth.

351

352

353

354

355

356

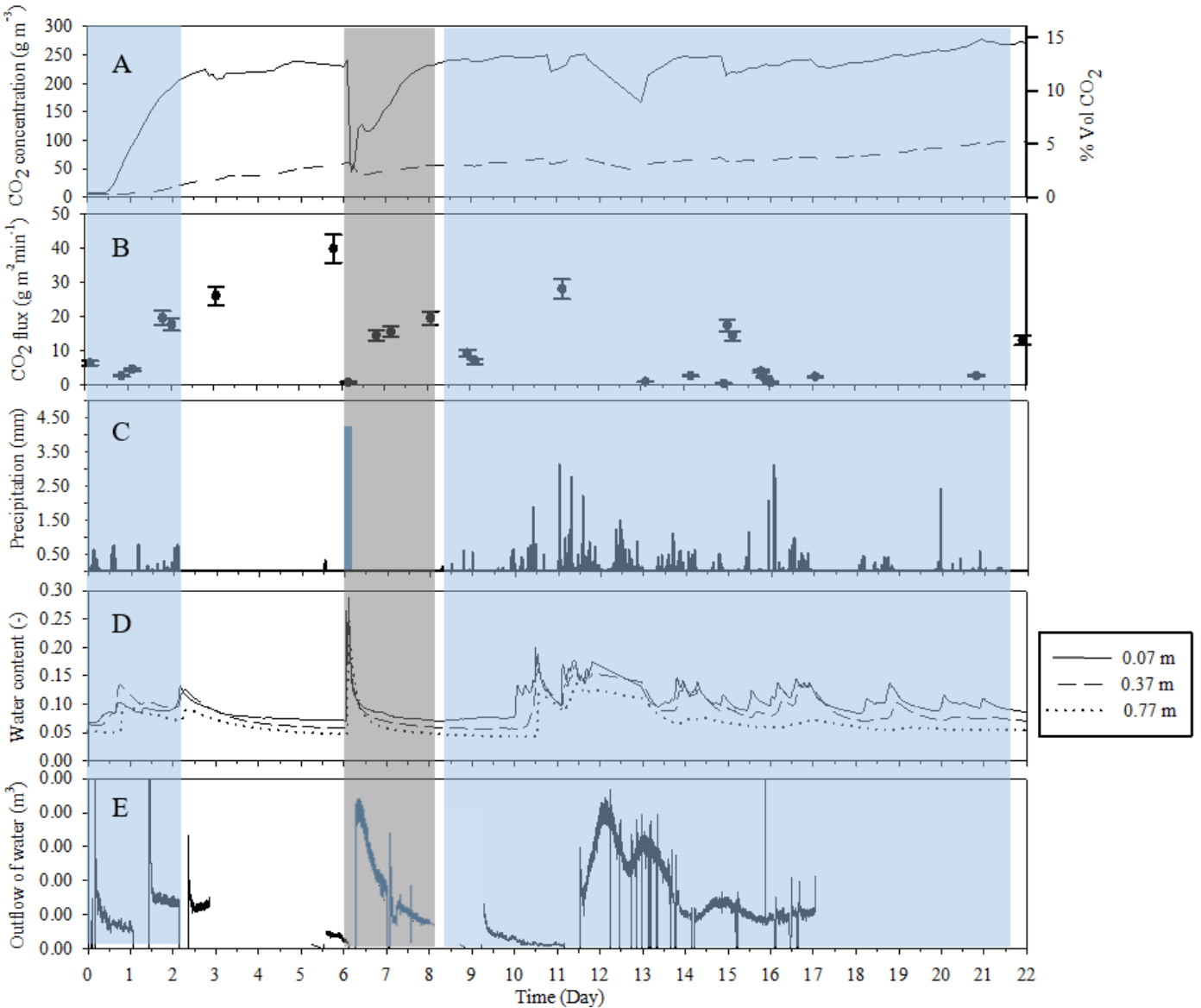


Figure 9. For the October experiment, times series of (A) CO₂ soil gas concentrations measured at 0.4 (solid line) and 0.8 m (short dash) depth, (B) CO₂ soil surface fluxes, in the centre of the lysimeter, (C) precipitation, the heavy rain are highlighted, (D) relative soil moisture at 0.07, 0.37 and 0.77 m depth and (E) outflow of water recorded during natural rainfall events from 8 d to 22 d of the October experiment. The data obtained after the artificial rainfall event are highlighted in grey.

357

358 The evolution of CO₂ soil gas concentrations and CO₂ fluxes at lysimeter surface during
 359 natural rainfall events are also shown in Figure 9. The evolution of CO₂ fluxes showed a
 360 relationship with the relative soil moisture (Figure 9-B, C and D) The CO₂ fluxes can be
 361 analysed between day 13 and 17 where enough measurements could be done (Figure 9-B).
 362 Between day 13 and 15, the effect of the heavy rainfall identified through the high water content

363 seem to lead to very low values of CO₂ fluxes (below 1 mg m⁻² min⁻¹), despite the still high CO₂
 364 concentrations in the soil. These values are even lower than the one observed during or after
 365 the artificial event. This may be linked to the higher water content than during the artificial
 366 event period. During a short period, at day 15, some values of significant fluxes, close to the
 367 one after the artificial rainfall event, are observed (≈ 17.5 mg m⁻² min⁻¹). They occur in a period
 368 where the soil water content decreases and reaches values close to the one observed after the
 369 rainfall event. However, when the water content increases again, the fluxes become negligible
 370 again. Despite few values a similar behaviour could be observed at day 21 and 22 where a
 371 decrease of water content seems to lead to high CO₂ fluxes values.

372 4. Discussion

373 4.1. Soil CO₂ diffusivities

374 During the artificial rainfall event, the increase of soil moisture content impacted CO₂
 375 soil gas fluxes. The Figure 10 shows the good accordance between CO₂ fluxes measurements
 376 and CO₂ concentration gradients calculated between 0 and 0.4 m depth at the beginning of the
 377 CO₂ injection until steady state.

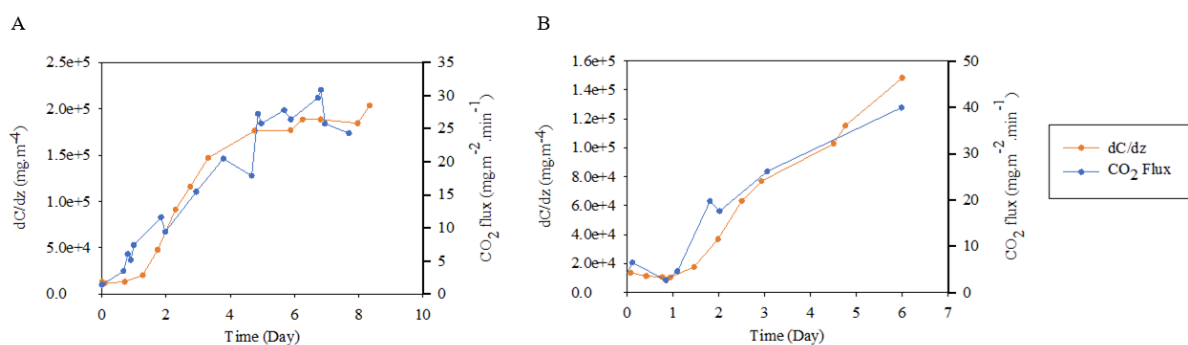


Figure 10. Relationship between CO₂ fluxes measurements and CO₂ concentration gradients (0 - 0.4 m depth) during February experiment (A) and October experiment (B).

378

379 According to first Fick law, the CO₂ flux (F_{CO_2}) and CO₂ concentration are related
 380 through the effective diffusion coefficient (D_e):

381 $F = D_e \times \frac{dc}{dz}$ (6)

382 Even if atmospheric pressure varied during the experiments, Atteia and Höhener (2010)
 383 showed that advective fluxes play a significant role only when the water saturation is very close
 384 one, which never occur during the experiment.

385 Therefore, the experimental D_e can be calculated using eq. 6 and results from Figure 10. For
 386 both experiment, D_e was calculated at steady state (8.5 and 6.0 d) and after the rainfall event
 387 (9.22 and 6.17 d) on the first 40 centimetres (Table 3). The experimental D_e were compared to
 388 the one predicted by classical empirical formulae in Table 3. Indeed, D_e can be estimated with
 389 the molecular diffusivity of CO_2 in air and an empirical tortuosity factors (τ) which was
 390 determined in function of gas-phase (Θ_g) and total (Θ) porosity. τ was estimated according to
 391 the relationships of Moldrup (2000) $\tau = \Theta_g^{2.5}/\Theta$, Millington and Quirk (1961) $\tau = \Theta_g^{10/3}/\Theta^2$,
 392 Millington (1959) $\tau = \Theta_g^{7/3}/\Theta^2$ and Penman (1940) $\tau = 0.66 \times \Theta_g$. These calculations were
 393 based on the experimental measurements (Figure 3).

394 Table 3. Effect of soil air-filled porosity on the measured effective diffusion coefficient and
 395 comparison with values calculated by empirical methods.

Experiment	1st		2nd	
	At steady state	After artificial rainfall event	At steady state	After artificial rainfall event
Soil moisture content (0 to 0.4 m depth) (-)	0.09	0.24	0.13	0.245
Experimental D_e ($\text{m}^2 \text{s}^{-1}$)	$2.35 \times 10^{-6} \pm 2.4 \times 10^{-7}$	$9.48 \times 10^{-7} \pm 9.7 \times 10^{-8}$	$4.66 \times 10^{-6} \pm 4.8 \times 10^{-7}$	$9.30 \times 10^{-8} \pm 9.5 \times 10^{-9}$
Moldrup et al. (2000)	1.19×10^{-6}	2.57×10^{-7}	7.53×10^{-7}	8.87×10^{-8}
Estimated D_e^a ($\text{m}^2 \text{s}^{-1}$)	Millington and Quirk (1961)	1.1×10^{-6}	4.17×10^{-8}	5.97×10^{-7}
	Millington (1959)	4.57×10^{-6}	4.63×10^{-7}	2.99×10^{-6}
	Penman (1940)	2.20×10^{-6}	8.26×10^{-7}	1.83×10^{-6}

396 ^aFree-air diffusion coefficient used for calculation were $D_{\text{air}} \text{CO}_2 = 1.39 \times 10^{-5} \text{ m}^2 \text{s}^{-1}$ (Pritchard and Currie, 1982)

397

398 As expected, D_e decreases with the increase of soil moisture content (Hers et al., 2000;
 399 Jassal et al., 2005). According to the 1st experiment results, at steady state (8.5 and 6 d), D_e was

400 about $2.35 \times 10^{-6} \text{ m}^2 \text{ s}^{-1}$ and decreased drastically after the artificial rainfall event (9.22 d) to
401 $9.48 \times 10^{-7} \text{ m}^2 \text{ s}^{-1}$. The same observation can be done for the 2nd experiment.

402 Overall, the comparisons between experimental and calculated D_e indicate that the
403 Penman and Millington (1959) relationships provide correct estimates. Indeed, the D_e were
404 similar or close by a factor of 0.55 to 2.55.

405 An exception was found for the estimated D_e , during the second experiment (after
406 artificial rainfall event), where the estimated D_e calculated with the Moldrup relationship
407 seemed approaching to experimental value with D_e of $8.87 \times 10^{-8} \text{ m}^2 \text{ s}^{-1}$ and $9.30 \times 10^{-8} \text{ m}^2 \text{ s}^{-1}$,
408 respectively.

409 Hers et al. (2000) also observed a difference of the same order of magnitude between
410 the measured and predicted values. They obtained a good comparison between the measured
411 gas-phase tortuosity factor and the one predicted using the Millington and Quirk relationship
412 with measured tortuosity factors about twice the predicted values.

413 These differences could be partly explained by the uncertainties in the experimental
414 measures on the CO₂ flux, soil moisture contents and soil CO₂ concentrations.

415 4.2.Influence of rainfall events

416 Few studies, to our knowledge, tried understanding the impacts of rainfall events on the
417 CO₂ leakages to the environment and more particularly their influence on the CO₂ diffusion
418 along soil profile and CO₂ fluxes (Oh et al., 2019; Seo et al., 2020). Understanding mechanisms
419 is however crucial to advance modelling approaches to simulate CO₂ flux surfaces under
420 changing environmental conditions.

421 4.2.1. Artificial rainfall event

422 After the artificial rainfall events, soil moisture content firstly increased while a
423 significant decrease of soil CO₂ concentrations and CO₂ fluxes was observed. After this, CO₂

424 concentrations and soil water contents reached back the steady state values at approximately 2
425 days. The recovery process was longer for CO₂ fluxes. However, for both experiments, the
426 return to the steady state of CO₂ fluxes was not observed. During the 1st experiment, it is
427 possible that the measurement was stopped before the end of the recovery step. For the 2nd
428 experiment, the heavy natural rainfall prevented the observation of the return to steady state.

429 A similar behaviour was observed by Lewicki et al. (2009) and Tommasone Pascale al.
430 (2015). During a CO₂ release experiment, Lewicki et al. (2009) observed a decrease of CO₂
431 concentration which could have been partially due to changes in soil physical properties
432 associated with significant rainfall events (10 – 20 mm). However, this effect of precipitations
433 was not observed on the CO₂ fluxes. Tommasone Pascale al. (2015) studied the effect of
434 rainstorm events on ²²²Rn activity in soil, and observed an immediate drop in ²²²Rn activities
435 by several orders of magnitude after rainfall events. At the end of precipitation, soil ²²²Rn
436 activities did not appear to recover rapidly, at least for a time span of about a couple of days
437 after storm ending. Tommasone Pascale et al (2015) shared the hypothesis given by Garcia-
438 Vindas and Monnin (2005) stating that the immediate drop in ²²²Rn activities following rainfall
439 events are attributed to the dissolution of ²²²Rn into the infiltrated water. This step consists in
440 the “wash-out step” during which rainfall water infiltrates into the pore network and
441 progressively washes out the radon, likely transferring to lower levels of the profile. Besides
442 the different chemical behaviour of ²²²Rn and CO₂ (e.g. production and decay), the present study
443 seems to support this hypothesis. Indeed, a clear decrease of the total CO₂ mass was observed
444 after the artificial rainfall event (Table 1).

445 In the mass balance calculations, the loss of CO₂ in the considered volume was like the
446 loss measured at the soil surface. This implies that there is no entering flux of CO₂ from the
447 source located below 80 cm while it is still providing a flux of CO₂. One potential explanation,
448 which is already cited by Viveiros et al. (2008), is that during a significant rainfall event the

449 soil gas is blocked below the infiltrated water. In that case, there could be a significant advective
450 downward soil gas flux that would prevent the arrival of high CO₂ gas from the source.

451 Concerning the slow recovery stage of gas concentrations, there was no explication or
452 hypothesis established in the literature at our knowledge. The results showed that the CO₂
453 profiles went overall back to steady state after 2.37 days from the beginning of rainfall event
454 for the 1st experiment and 1.87 days for the 2nd experiment (Figure 7). However, observation
455 data indicate that depending on depth CO₂ concentrations were not exactly back to steady state
456 at the same time. For example, during the 1st experiment, CO₂ concentration at 0.8 m depth was
457 back to steady state after about 2.46 and after 4.3 d at 0.4 m depth. The longer of recovery time
458 lag at shallow depth may explain the slow recovery process of CO₂ flux. It would have been
459 interesting to follow the temporal evolution of CO₂ concentrations at different depths between
460 the surface and 0.4 m depth to confirm the time lag effect.

461 4.2.2. Influence of natural rainfall events

462 During the 2nd experiment, different intensities of precipitation impacted CO₂ fluxes
463 differently. The low-amplitude rainfall events and short-lived (estimated at less than 1-2 mm)
464 cause a temporary mere wetting of the first centimetres of the ground surface which does not
465 or barely affects soil CO₂ concentrations and flux. On the contrary, significant rainfall events
466 (higher than 2 mm) appear to produce a clear decrease of CO₂ fluxes, owing by increase of soil
467 moisture content in deeper. Tommasone Pascale et al (2015) also observed the modifications
468 of ²²²Rn activities deriving from significant rainfall depend on rainfall duration, persistency,
469 and intensity.

470 5. Conclusion

471 The effect of rainfall events on soil gas flux was experimentally studied with lysimeter
472 experiments. Rainfall and soil moisture have caused significant modifications in soil CO₂

473 concentrations and flux during both experiments. During persistent and significant rainfall, the
474 results clearly show a significant decrease of CO₂ flux to atmosphere induced by rainfall
475 infiltration and consequential wash-out of the CO₂ present in the soil. After rainfall events, the
476 recovery processes of soil CO₂ concentrations and fluxes were found to be very slow after the
477 end of the artificial rainfall. Moreover, it can be expected that the temporal evolution of soil
478 CO₂ concentrations is markedly dependent on the rainfall history of the site (total rainfall
479 intensity, frequency and duration, intervals between rainfall events...) and the soil
480 hydrodynamic properties. It should be noted that these experiments simulated conditions with
481 high CO₂ concentrations like conditions encountered at CO₂ storage sites or petroleum-
482 contaminated sites with high degradation rates. The conclusions can perhaps not be generalized
483 to other sites with low CO₂ concentrations, e.g. in arid climates where water infiltration could
484 stimulate respiration. In the present case, respiration in the vadose zone was assumed to be low
485 and independent on moisture content.

486 Complementary studies are needed to understand and take into account all parameters
487 that drive CO₂ diffusion along soil profile and CO₂ fluxes at the soil-atmosphere interface.
488 Understanding these mechanisms is crucial in order to advance modelling approaches to predict
489 CO₂ surfaces flux under changing environmental conditions.

490

491 Acknowledgement

492 The authors would like to thank the partner companies of the INNOVASOL consortium
493 which permitted to realize this research project.

494

495

496 References

- 497
- 498 Atteia, O., Höhener, P., 2010. Semianalytical Model Predicting Transfer of Volatile Pollutants
499 from Groundwater to the Soil Surface. Environ. Sci. Technol. 44, 6228–6232.
500 <https://doi.org/10.1021/es903477f>
- 501 Beaubien, S.E., Jones, D.G., Gal, F., Barkwith, A.K.A.P., Braibant, G., Baubron, J.-C., Ciotoli,
502 G., Graziani, S., Lister, T.R., Lombardi, S., Michel, K., Quattrocchi, F., Strutt, M.H.,
503 2013. Monitoring of near-surface gas geochemistry at the Weyburn, Canada, CO₂-EOR
504 site, 2001–2011. Int. J. Greenh. Gas Control, The IEAGHG Weyburn-Midale CO₂
505 Monitoring and Storage Project 16, S236–S262.
506 <https://doi.org/10.1016/j.ijggc.2013.01.013>
- 507 Bekele, D.N., Naidu, R., Chadalavada, S., 2014. Influence of spatial and temporal variability
508 of subsurface soil moisture and temperature on vapour intrusion. Atmos. Environ. 88,
509 14–22. <https://doi.org/10.1016/j.atmosenv.2014.01.053>
- 510 Bernardo, C., Vries, D.F. de, 2011. Permanent shallow subsoil CO₂ flux chambers for
511 monitoring of onshore CO₂ geological storage sites. Int. J. Greenh. Gas Control, The
512 5th Trondheim Conference on CO₂ Capture, Transport and Storage 5, 565–570.
513 <https://doi.org/10.1016/j.ijggc.2010.05.011>
- 514 Bornemann, F., 1920. Kohlensäure und Pflanzenwachstum. Mitt. Dtsch. Landwirtsch.-Ges.
515 35:363.
- 516 Choi, J.-W., Smith, J.A., 2005. Geoenvironmental Factors Affecting Organic Vapor Advection
517 and Diffusion Fluxes from the Unsaturated Zone to the Atmosphere under Natural
518 Conditions. Environ. Eng. Sci. 22, 95–108. <https://doi.org/10.1089/ees.2005.22.95>
- 519 Conant, B.H., Gillham, R.W., Mendoza, C.A., 1996. Vapor Transport of Trichloroethylene in
520 the Unsaturated Zone: Field and Numerical Modeling Investigations.
521 <https://doi.org/10.1029/95WR02965>
- 522 Cotel, S., Schaefer, G., Sylvie, T., Marzougui-Jaafar, S., Gay, G., Razakarisoa, O., 2015.
523 Evaluation of VOC fluxes at the soil-air interface using different flux chambers and a
524 quasi-analytical approach. Water. Air. Soil Pollut. 226. <https://doi.org/10.1007/s11270-015-2596-y>
- 525 Elío, J., Nisi, B., Ortega, M.F., Mazadiego, L.F., Vaselli, O., Grandia, F., 2013. CO₂ soil flux
526 baseline at the technological development plant for CO₂ injection at Hontomin (Burgos,
527 Spain). Int. J. Greenh. Gas Control 18, 224–236.
528 <https://doi.org/10.1016/j.ijggc.2013.07.013>
- 529 Elío, J., Ortega, M.F., Nisi, B., Mazadiego, L.F., Vaselli, O., Caballero, J., Chacón, E., 2016. A
530 multi-statistical approach for estimating the total output of CO₂ from diffuse soil
531 degassing by the accumulation chamber method. Int. J. Greenh. Gas Control 47, 351–
532 363. <https://doi.org/10.1016/j.ijggc.2016.02.012>
- 533 Fa, K.-Y., Liu, J.-B., Zhang, Y.-Q., Wu, B., Qin, S.-G., Feng, W., Lai, Z.-R., 2015. CO₂
534 absorption of sandy soil induced by rainfall pulses in a desert ecosystem. Hydrol.
535 Process. 29, 2043–2051. <https://doi.org/10.1002/hyp.10350>
- 536 Garcia-Vindas, J.R., Monnin, M.M., 2005. Radon concentration measurements in the presence
537 of water and its consequences for Earth sciences studies. Radiat. Meas. 39, 319–322.
538 <https://doi.org/10.1016/j.radmeas.2004.06.014>
- 539 Hers, I., Li, L., Hannam, S., 2004. Evaluation of soil gas sampling and analysis techniques at a
540 former petrochemical plant site. Environ. Technol. 25, 847–860.
541 <https://doi.org/10.1080/09593330.2004.9619377>

- 543 Hers, I., Zapf-Gilje, R., Li, L., Atwater, J., 2000. Measurement of in Situ Gas-Phase Diffusion
544 Coefficients. Environ. Technol. 21, 631–640.
545 <https://doi.org/10.1080/09593330.2000.9618948>
- 546 Jassal, R., Black, A., Novak, M., Morgenstern, K., Nesic, Z., Gaumont-Guay, D., 2005. Relationship between soil CO₂ concentrations and forest-floor CO₂ effluxes. Agric.
547 For. Meteorol. 130, 176–192. <https://doi.org/10.1016/j.agrformet.2005.03.005>
- 548 Kim, J., Yu, S., Yun, S.-T., Kim, K.-H., Kim, J.-H., Shinn, Y.-J., Chae, G., 2019. CO₂ leakage
549 detection in the near-surface above natural CO₂-rich water aquifer using soil gas
550 monitoring. Int. J. Greenh. Gas Control 88, 261–271.
551 <https://doi.org/10.1016/j.ijggc.2019.06.015>
- 552 Klenbusch, M., 1986. Measurement of Gaseous Emission Rates From Land Surfaces Using an
553 Emission Isolation Flux Chamber: User's Guide. US Environ. Prot. Agency Wash. DC
554 EPA6008-86008.
- 555 Lelli, M., Raco, B., 2017. A reliable and effective methodology to monitor CO₂ flux from soil:
556 The case of Lipari Island (Sicily, Italy). Appl. Geochem. 85, 73–85.
557 <https://doi.org/10.1016/j.apgeochem.2017.08.004>
- 558 Lewicki, J.L., Hilley, G.E., Dobeck, L., Spangler, L., 2009. Dynamics of CO₂ fluxes and
559 concentrations during a shallow subsurface CO₂ release. Environ. Earth Sci.
560 Ma, J., Zheng, X.-J., Li, Y., 2012. The response of CO₂ flux to rain pulses at a saline desert.
561 Hydrol. Process. 26, 4029–4037. <https://doi.org/10.1002/hyp.9204>
- 562 Matthias, A.D., Blackmer, A.M., Bremner, J.M., 1980. A Simple Chamber Technique for Field
563 Measurement of Emissions of Nitrous Oxide from Soils. J. Environ. Qual. 9, 251–256.
564 <https://doi.org/10.2134/jeq1980.00472425000900020017x>
- 565 Millington, R.J., 1959. Gas Diffusion in Porous Media. Science 130, 100–102.
566 <https://doi.org/10.1126/science.130.3367.100-a>
- 567 Millington, R.J., Quirk, J.P., 1961. Permeability of porous solids. Trans. Faraday Soc. 57, 1200–
568 1207. <https://doi.org/10.1039/TF9615701200>
- 569 Moldrup, P., Olesen, T., Gamst, J., Schjønning, P., Yamaguchi, T., Rolston, D.E., 2000. Predicting the Gas Diffusion Coefficient in Repacked Soil Water-Induced Linear
570 Reduction Model. Soil Sci. Soc. Am. J. 64, 1588–1594.
571 <https://doi.org/10.2136/sssaj2000.6451588x>
- 572 Norman, J.M., Kucharik, C.J., Gower, S.T., Baldocchi, D.D., Crill, P.M., Rayment, M., Savage,
573 K., Striegl, R.G., 1997. A comparison of six methods for measuring soil-surface carbon
574 dioxide fluxes. J. Geophys. Res. Atmospheres 102, 28771–28777.
575 <https://doi.org/10.1029/97JD01440>
- 576 Oh, Y.Y., Yun, S.T., Yu, S., Kim, H.J., Jun, S.C., 2019. A novel wavelet-based approach to
577 characterize dynamic environmental factors controlling short-term soil surface CO₂
578 flux: Application to a controlled CO₂ release test site (EIT) in South Korea. Geoderma
579 337, 76–90. <https://doi.org/10.1016/j.geoderma.2018.09.017>
- 580 Palaia, T., Jimmo, A., Mahler, N., Molinari, C., Clements, L., 2018. Technical measurement
581 guidance for LNAPL natural source zone depletion. CRC CARE Tech. Rep. No 44 254.
582 <https://doi.org/10.1089/ees.2005.22.95>
- 583 Penman, H.L., 1940. Gas and vapour movements in the soil: I. The diffusion of vapours through
584 porous solids. J. Agric. Sci. 30, 437–462. <https://doi.org/10.1017/S0021859600048164>
- 585 Petersen, L.W. (Danish I. of P. and S.S., El-Farhan, Y.H., Moldrup, P., Rolston, D.E.,
586 Yamaguchi, T., 1996. Transient diffusion, adsorption, and emission of volatile organic
587 vapors in soils with fluctuating low water contents. J. Environ. Qual. USA.
588 Reinhart, D.R., Cooper, D.C., Walker, B.L., 1992. Flux Chamber Design and Operation for the
589 Measurement of Municipal Solid Waste Landfill Gas Emission Rates. J. Air Waste
590 Manag. Assoc. 42, 1067–1070. <https://doi.org/10.1080/10473289.1992.10467053>
- 591
- 592

- 593 Risk, D.A., Kellman, L.M., Beltrami, H., 2002. Soil CO₂ production and surface flux at four
594 climate observatories in eastern Canada. <https://doi.org/10.1029/2001GB001831>
- 595 Rochette, P., Hutchinson, G., 2005. Measurement of Soil Respiration in situ: Chamber
596 Techniques. Publ. USDA-ARS UNL Fac.
- 597 Rodier, J., 1976. L'analyse de l'eau. Eaux naturelles, eaux résiduaires, eaux de mer., Dunod
598 Tech, Bordas, Paris. ed.
- 599 Sander, S.P., Friedl, R.R., Barker, J.R., Abbatt, J.P.D., Burkholder, J.B., Friedl, R.R., Golden,
600 D.M., Huie, R.E., Kolb, C.E., Kurylo, M.J., Moortgat, G.K., Orkin, V.L., Wine, P.H.,
601 2011. Chemical Kinetics and Photochemical Data for Use in Atmospheric Studies
602 Evaluation No. 17. JPL Publ. 10–6, Jet Propulsion Laboratory, Pasadena, 684.
- 603 Schroder, I.F., Zhang, H., Zhang, C., Feitz, A.J., 2016. The role of soil flux and soil gas
604 monitoring in the characterisation of a CO₂ surface leak: A case study in Qinghai,
605 China. Int. J. Greenh. Gas Control 54, 84–95.
606 <https://doi.org/10.1016/j.ijggc.2016.07.030>
- 607 Seo, D.H., Han, W.S., Park, E., Jeong, J., Oh, Y.-Y., Kim, H.-J., Yoo, G., Jun, S.-C., Yun, S.-
608 T., 2020. Analyses and numerical evaluation of integrated time-series monitoring
609 datasets including CO₂ concentration and fluxes at controlled CO₂ release site in South
610 Korea. J. Hydrol. 590, 125213. <https://doi.org/10.1016/j.jhydrol.2020.125213>
- 611 Shao, H., Ussiri, D.A.N., Patterson, C.G., Locke, R.A., II, Wang, H., Taylor, A.H., Cohen, H.F.,
612 2019. Soil gas monitoring at the Illinois Basin – Decatur Project carbon sequestration
613 site. Int. J. Greenh. Gas Control 86, 112–124.
614 <https://doi.org/10.1016/j.ijggc.2019.04.012>
- 615 Shen, R., Pennell, K.G., Suuberg, E.M., 2013. Influence of Soil Moisture on Soil Gas Vapor
616 Concentration for Vapor Intrusion. Environ. Eng. Sci. 30, 628–637.
617 <https://doi.org/10.1089/ees.2013.0133>
- 618 Shen, R., Pennell, K.G., Suuberg, E.M., 2012. A numerical investigation of vapor intrusion--
619 the dynamic response of contaminant vapors to rainfall events. Sci. Total Environ. 437,
620 110–120. <https://doi.org/10.1016/j.scitotenv.2012.07.054>
- 621 Smith, J.A., Tisdale, A.K., Cho, H.J., 1996. Quantification of Natural Vapor Fluxes of
622 Trichloroethene in the Unsaturated Zone at Picatinny Arsenal, New Jersey. Environ.
623 Sci. Technol. 30, 2243–2250. <https://doi.org/10.1021/es950610c>
- 624 Tillman, F.D., Smith, J.A., 2004. Design and laboratory testing of a chamber device to measure
625 total flux of volatile organic compounds from the unsaturated zone under natural
626 conditions. J. Contam. Hydrol. 75, 71–90.
627 <https://doi.org/10.1016/j.jconhyd.2004.04.005>
- 628 Tommasone Pascale, F., Carbone, P., De Francesco, S., Cuoco, E., Tedesco, D., 2015. Rainstorm-induced soil 222Rn concentration spikes observed in Southern Italy.
629 Environ. Earth Sci. 73, 8177–8187. <https://doi.org/10.1007/s12665-014-3976-0>
- 630 Viveiros, F., Ferreira, T., Cabral Vieira, J., Silva, C., Gaspar, J.L., 2008. Environmental
631 influences on soil CO₂ degassing at Furnas and Fogo volcanoes (São Miguel Island,
632 Azores archipelago). J. Volcanol. Geotherm. Res., Volcanic Flows and Falls 177, 883–
633 893. <https://doi.org/10.1016/j.jvolgeores.2008.07.005>
- 634 Werner, D., Grathwohl, P., Höhener, P., 2004. Review of Field Methods for the Determination
635 of the Tortuosity and Effective Gas-Phase Diffusivity in the Vadose Zone. Vadose Zone
636 J. 3, 1240–1248. <https://doi.org/10.2136/vzj2004.1240>
- 637 Wilke, B.-M., 2005. Determination of Chemical and Physical Soil Properties, in: Margesin, R.,
638 Schinner, F. (Eds.), Monitoring and Assessing Soil Bioremediation, Soil Biology.
639 Springer, Berlin, Heidelberg, pp. 47–95. https://doi.org/10.1007/3-540-28904-6_2
- 640 Yang, L., Chen, Z., Zhang, X., Liu, Y., Xie, Y., 2015. Comparison study of landfill gas
641 emissions from subtropical landfill with various phases: A case study in Wuhan, China.
- 642

643 J. Air Waste Manag. Assoc. 65, 980–986.
644 https://doi.org/10.1080/10962247.2015.1051605
645